

# Analysis of high-field side plasma instabilities in tokamak edge

M.V. Umansky

*Lawrence Livermore National Laboratory, Livermore, CA 94550, USA*

## Abstract

Balanced double-null configurations are of general interest for boundary plasma physics, and they have been proposed for some future designs. Experimental observations demonstrate absence of plasma fluctuations in tokamak high-field side scrape-off layer in a balanced double-null configuration [Smick et al 2013 Nucl. Fusion 53 023001], and it is commonly assumed that plasma instabilities are suppressed on high-field side in the edge plasma due to the stabilizing effect of magnetic curvature. At the same time, the experimental evidence points to extremely steep plasma density profiles on high-field side, which should provide a strong instability drive. In the present study, the drift-resistive-balloonning mode instability model is investigated analytically and numerically to determine the characteristics of plasma instabilities, turbulence, and transport in tokamak scrape-off layer on high-field side.

*Keywords:*

## 1. Introduction

Tokamak balanced double-null (DN) configurations are of general interest for boundary plasma physics, and they have been proposed for some future designs such as ARIES [1], FDF [2], ARC [3], EU-DEMO [4], and others. One reason such configurations are attractive is that using two outer divertors may simplify dealing with the exhaust power. Another attractive feature is that in balanced DN configurations the scrape-off-layer (SOL) plasma on high-field side (HFS) has been found to be quiescent, unlike the low-field side (LFS), and placing radio-frequency (RF) actuators on HFS may be more efficient due to expectation of low scattering in the SOL on HFS [5].

The subject of this study is analysis of plasma linear stability and turbulence in the SOL on the HFS of a tokamak, in particular for near-balanced DN magnetic configurations when the HFS SOL does not directly connect to the LFS SOL.

For a balanced DN configuration, the LFS and HFS of the SOL are essentially the same in terms of physics. Topologically it is a slab-like domain with toroidal and poloidal magnetic field; the difference between the LFS and HFS SOL is basically in the direction of the magnetic curvature vector with respect to the plasma density and pressure gradient, which makes the magnetic curvature destabilizing on LFS and stabilizing on HFS.

There are many experimental observations of LFS SOL on different tokamaks, indicating ubiquitous presence of turbulent fluctuations and transport. For the HFS, there are very few measurements. Probably the best diagnosed HFS SOL is in Alcator C-Mod, where scanning Langmuir probe measurements were carried out on HFS [6–8]. The main observations from those studies for balanced DN con-

figurations were that (i) HFS SOL is extremely narrow, and (ii) the level of fluctuations and fluctuations-induced radial particle flux on HFS is very low. Theoretical analysis of these observations is the subject of the present study.

## 2. Physics model

For the model of plasma instabilities in tokamak SOL we use the following plasma fluid equations:

Density conservation

$$\frac{\partial N_i}{\partial t} = -\vec{V}_E \cdot \nabla N_i \quad (1)$$

Charge conservation (potential vorticity)

$$\frac{\partial \varpi}{\partial t} = -\vec{V}_E \cdot \nabla \varpi - 2\omega_{ci} \vec{b} \times \kappa \cdot \nabla P_{ei} - N_i Z_i e \frac{4\pi V_A^2}{c^2} \nabla_{||} j_{||} \quad (2)$$

Electron parallel momentum

$$\frac{e}{m_e} E_{||} + \frac{1}{N_i m_e} (T_e \partial_{||} N_i) = 0.51 \nu_{ei} (V_{||i} - V_{||e}) \quad (3)$$

where

$$\begin{aligned} \varpi &= N_i e \nabla_{\perp}^2 \phi \\ \vec{V}_E &= c \vec{b}_0 \times \nabla_{\perp} \phi / B \\ E_{||} &= -\partial_{||} \phi \\ \nabla_{||} F &= B \partial_{||} (F/B) \end{aligned}$$

Eqs. (1,2,3), with some variations, form the basis of many theoretical studies of tokamak edge turbulence, pioneered in the early 1990s by Guzdar et al. [9]. As these equations support drift-resistive and ballooning instabilities this physics model is often called the drift-resistive-balloonning mode (DRBM). Here the DRBM model is analyzed in a double-periodic slab geometry sketched in Fig. (1);  $x, y, z$  are the field-aligned coordinates described, e.g., in Ref. ([10]).

### 3. Linear analysis

#### 3.1. Linearized equations

We assume uniform background temperature  $T_{e0}=\text{const}$ , for the background plasma density assume constant radial gradient scale length  $\nabla N_{i0} = N_{i0}/L_n$ , no background ion flow,  $V_{||i} = 0$ , no background electric potential,  $\phi_0 = 0$ , and weakly varying background magnetic field  $B$ . We assume constant curvature in the negative radial direction,  $\vec{\kappa} = -\hat{e}_x/R$ , and  $\vec{b} \times \kappa$  perpendicular to the field within flux surface in the positive  $\nabla z$  direction (see the geometry sketch). Then in the field-aligned  $(x, y, z)$  coordinates (both  $y$  and  $z$  are periodic) the operator  $\vec{b} \times \kappa \cdot \nabla$  appears to be  $(1/R)\nabla_z$ . For details of differential operators in the field-aligned coordinates see, e.g., Ref. ([10]).

Then the linearized Fourier-decomposed equations are

$$-i\omega\tilde{N}_i = -\frac{ick_{\perp}}{B} \frac{N_{i0}}{L_n} \tilde{\phi} \quad (4)$$

$$\begin{aligned} -i\omega N_{i0} e k_{\perp}^2 \tilde{\phi} &= 2\Omega_{ci} T_{e0} \frac{1}{R_c} i k_{\perp} \tilde{N}_i + \\ &+ (N_{i0} e)^2 \frac{4\pi V_A^2}{c^2} i k_{||} \tilde{V}_{||e} \end{aligned} \quad (5)$$

$$0 = \frac{e}{m_e} i k_{||} \tilde{\phi} - \frac{T_{e0}}{N_{i0} m_e} i k_{||} \tilde{N}_i - 0.51 \nu_{ei} \tilde{V}_{||e} \quad (6)$$

#### 3.2. Linear dispersion relation

The linearized Fourier-decomposed equations (using ion charge  $Z_i=1$ ) lead to the dispersion relation

$$\omega^2 + \Omega_K^2 + i\sigma_{||}(\omega - \omega_*) = 0 \quad (7)$$

where the standard textbook [11] notation is used,

$$\sigma_{||} = \left( \frac{k_{||}}{k_{\perp}} \right)^2 \frac{\Omega_{ci} \omega_{ce}}{0.51 \nu_{ei}} \quad (8)$$

$$\omega_{*e} = k_{\perp} V_{*e} = k_{\perp} \frac{V_{te}^2}{\omega_{ce} L_n} \quad (9)$$

$$\Omega_K^2 = \pm \frac{2C_s^2}{RL_n} \quad (10)$$

$$C_s^2 = T_{e0}/M_i \quad (11)$$

$$V_{te}^2 = T_{e0}/m_e \quad (12)$$

Due to the relative orientation of the magnetic curvature and the SOL density gradient, on LFS the curvature term is positive,  $\Omega_K^2 > 0$ ; and on HFS it is negative,  $\Omega_K^2 < 0$ .

#### 3.3. Solution of linear dispersion relation

Normalizing each term in the dispersion relation by  $\omega_*$  we obtain

$$\hat{\omega}^2 + \hat{\Omega}_K^2 + i\hat{\sigma}_{||}(\hat{\omega} - 1) = 0 \quad (13)$$

This is a quadratic equation, and analyzing the coefficients one can see that for  $\hat{\Omega}_K^2 \geq 0$  the equation always has an unstable solution as it has one root above and one below the real axis. Indeed,

$$\hat{\omega}_1 + \hat{\omega}_2 = -i\hat{\sigma}_{||} \quad (14)$$

so the real parts of roots are opposite.

Next, using  $\hat{\omega}_1 = a + bi$ ,  $\hat{\omega}_2 = -a + ci$ , where  $a, b, c$  are real, we find

$$\hat{\omega}_1 \hat{\omega}_2 = (-a^2 - bc) + (ac - ab)i = \hat{\Omega}_K^2 - i\hat{\sigma}_{||}, \quad (15)$$

so

$$bc = -a^2 - \hat{\Omega}_K^2 \quad (16)$$

For  $\hat{\Omega}_K^2 > 0$  (on LFS) the product  $bc$  must be negative; in other words, the imaginary parts of the two roots have opposite sign, so there is always one stable and one unstable root. However, for  $\hat{\Omega}_K^2 < 0$  (on HFS) it can happen that there is no unstable root, depending on the size of the curvature term. Using  $\hat{\Omega}_K^2 = -1$  in the dispersion relation Eq. (13), one can rewrite it as

$$(\hat{\omega} - 1)(\hat{\omega} + 1 + i\hat{\sigma}_{||}) = 0, \quad (17)$$

so one can see that this is a marginal situation when one root is on the real axis and the other one in the lower half of the complex plane. For  $\hat{\Omega}_K^2 < -1$  both roots are in the lower-half of the complex plane, so there is no unstable solution anymore. On the other hand, for  $-1 < \hat{\Omega}_K^2 < 0$  there is still an unstable root, but the growth rate is reduced by the curvature.

Next, defining the collisionality parameter

$$\mathcal{A} = \frac{1}{0.51} \sqrt{\frac{M}{m}} (k_{||}^2 \lambda_{ei} L_n), \quad (18)$$

the curvature parameter

$$\mathcal{B} = \sqrt{\frac{2L_n}{R}}, \quad (19)$$

and the normalized nondimensional wavenumber

$$\xi_{\perp} = k_{\perp} \rho_{ci}, \quad (20)$$

one can write the dispersion relation Eq. (13) as

$$\hat{\omega}^2 + i \frac{\mathcal{A}}{\xi_{\perp}^3} \hat{\omega} + \frac{\mathcal{B}^2}{\xi_{\perp}^2} - i \frac{\mathcal{A}}{\xi_{\perp}^3} = 0 \quad (21)$$

The solutions of Eq. (21) are shown in Fig. (2) where the instability growth rate  $Im(\hat{\omega})$  is plotted against  $\xi_{\perp}$  for several values of parameters  $\mathcal{A}, \mathcal{B}$ . One can see in the Fig. (2) that depending on the parameters  $\mathcal{A}, \mathcal{B}$  there is a window of instability. For negative  $\mathcal{B}^2$  the growth rate is reduced compared to the no-curvature case  $\mathcal{B} = 0$ , and there is a cut-off value  $\xi_{\perp} = |\mathcal{B}|$  below which the instability is suppressed.

#### 4. Numerical simulations

Numerical solutions of Eqs. (1,2,3) is carried out with SOLT3D [12] which is a plasma simulation code implemented in the BOUT++ framework [13]. Similar to the linear analysis, the numerical calculations are performed in the slab geometry using field-aligned coordinates sketched in Fig. (1), where both  $y$  and  $z$  coordinates are periodic.

First, we verify the linear dispersion relation in the code. Figure (3) shows the solution to Eq. (21) and the results from SOLT3D, which appear in full consistency, for a particular choice of parameters  $\mathcal{A}=468$  and  $\mathcal{B}^2=-8.9$  where the local theory is valid. Note that for C-Mod DN HFS, the relevant values of the nondimensional parameters would be  $\mathcal{A} \approx 0.1$  and  $\mathcal{B}^2 \approx -0.003$ , using  $L_n = 0.1$  cm,  $R = 70$  cm,  $\lambda_{ei} = 10$  cm,  $k_{\parallel} = 0.03$  cm $^{-1}$ , estimated from experimental data in Ref. [6].

Next, nonlinear simulations are carried out where the system relaxes to saturated turbulence. This is still done for shallow radial plasma profiles, far from the experimental situation where the plasma density drops rapidly across the separatrix resulting in an extremely thin scrape-off layer on the HFS with very sharp radial plasma profiles in balanced double-null [6, 8]. However, with the chosen parameters, the system is much more tractable for both analytic treatment and the simulations, which still allows capturing some important features of tokamak plasma on HFS; extending the analysis to realistic HFS plasma profiles is a planned extension of the present study.

For the present numerical simulations, the parameters are:  $R=1$  m,  $T_{e0}=100$  eV,  $N_{i,sep}=0.5 \times 10^{20}$  m $^{-3}$ ,  $B_t=1$  T,  $B_p=0.1$  T. Three cases are considered, with  $L_n=2.25$  m, 1.125 m, and 0.5625 m.

In the numerical simulations, the average plasma density profile is maintained fixed while the electric potential and vorticity profiles evolve freely. The system evolving in time goes through the linear growth phase and settles in a steady turbulence state.

One quantity of primary interest in the simulations is the radial density flux  $\Gamma_x$  in the steady turbulence state.

We calculate  $\Gamma_x$  for three different values of the plasma density scale length  $L_n$ . It is found that the fluctuations amplitude and the time-average flux  $\langle \Gamma_x \rangle$  grow strongly with  $1/L_n$ , see Fig. (4) where the symbols show the results from the simulations, the dashed line shows the power-law fit  $\Gamma = 3 \times 10^{14}/L_n^4$  and the dot-dashed line shows the exponential fit  $\Gamma = 4 \times 10^{12} \exp(4/L_n)$  (in MKS units).

Another interesting observation is that the probability distribution function (PDF) of  $\Gamma_x$  undergoes significant changes as  $1/L_n$  grows, going from nearly symmetric distribution to a strongly skewed one, see Fig. (5)

#### 5. Discussion

The strong dependence of the turbulent radial flux  $\Gamma_x$  on the plasma density radial scale length  $L_n$  suggests that the radial plasma profile is governed by marginal stability physics, so the resulting level of fluctuations may be small.

Indeed, for the plasma profile at the separatrix, one can make an estimate from the condition  $\nabla \cdot \vec{\Gamma} \approx 0$ ,

$$\frac{\Gamma_x}{L_n} \sim \frac{C_s N_i}{L_{\parallel}}, \quad (22)$$

so for an equilibrium one needs

$$\Gamma_x = \alpha L_n, \quad (23)$$

where  $\alpha = C_s N_i / L_{\parallel}$  is a numerical factor.

On the other hand, the numerical results in Fig. (4) show rapid growth of  $\Gamma_n$  with  $1/L_n$ , which can be approximated, e.g., by an exponential scaling,

$$\Gamma_x = \beta \exp(\lambda / L_n), \quad (24)$$

where  $\beta, \lambda$  are numerical factors.

Thus, the equilibrium density scale length  $L_n$  is defined by the solution to the equation

$$\alpha L_n = \beta \exp(\lambda / L_n), \quad (25)$$

which has a single root, and the resulting  $L_n$  (and the corresponding level of turbulent fluctuations) will depend on the numerical values of parameters  $\alpha, \beta$ , and  $\lambda$ . Of course, based on the present simulations with  $L_n \sim 1$  m it would be meaningless to extrapolate to realistic  $L_n \sim 1$  mm.

The changes of  $\Gamma_x$  PDF with  $L_n$  shown in Fig. (5) is an interesting feature suggesting coupling of unstable and damped modes in the steady state turbulence. It is known that stable (damped) modes may play a significant role in plasma turbulence [14]. One can make an argument in the spirit of the quasilinear plasma theory, noticing that unstable modes correspond to radially outward radial plasma density flux while the damped modes correspond to radially inward density flux.

Indeed, consider the linearized density evolution equation, Eq. (4), in the Fourier decomposed form,

$$-i\omega\tilde{N}_i = \tilde{V}_E N_{i0}/L_n, \quad (26)$$

Then,

$$\tilde{V}_E = -i\omega(L_n/N_{i0})\tilde{N}_i, \quad (27)$$

and assuming that the mode beats with itself, for the average density flux we find,

$$\langle\Gamma_x\rangle = \frac{1}{2}Re(\tilde{N}_i\tilde{V}_E^*) = \frac{1}{2}|\tilde{N}_i|^2(L_n/N_{i0})\gamma \quad (28)$$

where  $\gamma = Im(\omega)$  is the mode growth rate.

Thus, unstable modes give rise to outward radial density flux and damped modes give rise to inward flux, which may be relevant to the  $\Gamma_x$  PDF in Fig. (5). Indeed, as can be seen from the linear analysis, the instability domain corresponds to  $k_{\perp}\rho_{ci} > \sqrt{2L_n/R}$ ; so, for large  $L_n$  there is a large pool of damped modes. Consistent with that, as Fig. (5) shows, for large  $L_n$  there is a significant contribution of negative fluctuations of turbulent flux.

It is interesting to note that for the parameters used in the present numerical simulations, the turbulent flux on LFS is orders of magnitude higher than that on HFS. This is not too surprising, given that on LFS the stabilizing curvature term becomes destabilizing and there is robust instability for all wavenumbers.

## 6. Conclusions

Linear and nonlinear analysis is conducted using the DRBM instability model for tokamak SOL plasma on HFS in a balanced DN configuration where the magnetic curvature has stabilizing effect. Experimental evidence on HFS points to absence of fluctuations and to steep radial gradients of plasma density and pressure on the separatrix. On the other hand, the present analysis indicates that steep gradients should favor the instability drive over the magnetic curvature stabilization, and some level of fluctuations must be present on HFS, although the amplitude may be small due to marginal stability type constraints. For quantitative comparison with the experiment, apparently a more complete model will be needed, using realistic radial plasma profiles. Furthermore, the extended model should include mechanisms that may suppress the instability, such as the finite Larmor radius (FLR) effects, the strongly varying background radial electric field, and the X-point geometry with magnetic field shearing. In view of the ideas to place RF actuators on the tokamak HFS [5], an important question for further investigation is whether edge plasma fluctuations can be destabilized on HFS by the RF antenna field.

## Acknowledgements

The author gratefully acknowledges discussions with B. I. Cohen and J. R. Myra. This work was performed under the auspices of the US Department of Energy by Lawrence Livermore National Security, LLC, Lawrence Livermore National Laboratory, under Contract DE-AC52-07NA27344.

## References

[1] F. Najmabadi, R. Conn, C. Bathke, L. Bromberg, E. Cheng, D. Cohn, P. Cooke, R. Creedon, D. Ehst, K. Evans, N. Ghoniem, S. Grotz, M. Hasan, J. Hogan, J. Herring, A. Hyatt, E. Ibrahim, S. Jardin, C. Kessel, M. Klasky, R. Krakowski, T. Kunugi, J. Leuer, J. Mandrekas, R. Martin, T.-K. Mau, R. Miller, Y.-K. Peng, R. Reid, J. Santarius, M. Schaffer, J. Schultz, K. Schultz, J. Schwartz, S. Sharafat, C. Singer, L. Snead, D. Steiner, D. Strickler, D.-K. Sze, M. Valenti, D. Ward, J. Williams, L. Wittenberg, C. Wong, The aries-i tokamak reactor study, in: B. KEEN, M. HUGUET, R. HEMSWORTH (Eds.), *Fusion Technology 1990*, Elsevier, Oxford, 1991, pp. 253–257. doi: <https://doi.org/10.1016/B978-0-444-88508-1.50033-5>. URL <https://www.sciencedirect.com/science/article/pii/B9780444885081500335>

[2] V. S. Chan, R. D. Stambaugh, A. M. Garofalo, M. S. Chu, R. K. Fisher, C. M. Greenfield, D. A. Humphreys, L. L. Lao, J. A. Leuer, T. W. Petrie, R. Prater, G. M. Staebler, P. B. Snyder, H. E. S. John, A. D. Turnbull, C. P. C. Wong, M. A. V. Zeeland, Physics basis of a fusion development facility utilizing the tokamak approach, *Fusion Science and Technology* 57 (1) (2010) 66–93. arXiv:<https://doi.org/10.13182/FST10-A9269>. doi:10.13182/FST10-A9269. URL <https://doi.org/10.13182/FST10-A9269>

[3] A. Kuang, N. Cao, A. Creely, C. Dennett, J. Hecla, B. LaBombard, R. Tinguely, E. Tolman, H. Hoffman, M. Major, J. Ruiz Ruiz, D. Brunner, P. Grover, C. Laughman, B. Sorbom, D. Whyte, Conceptual design study for heat exhaust management in the arc fusion pilot plant, *Fusion Engineering and Design* 137 (2018) 221–242. doi:<https://doi.org/10.1016/j.fusengdes.2018.09.007>. URL <https://www.sciencedirect.com/science/article/pii/S0920379618306185>

[4] L. Aho-Mantila, F. Subba, D. Coster, L. Xiang, F. Militello, T. Lunt, D. Moulton, H. Reimerdes, M. Wensing, M. Wischmeier, R. Ambrosino, X. Bonnin, M. Siccinio, Scoping the characteristics and benefits of a connected double-null configuration for power exhaust in eu-demo, *Nuclear Materials and Energy* 26 (2021) 100886. doi:<https://doi.org/10.1016/j.nme.2020.100886>. URL <https://www.sciencedirect.com/science/article/pii/S2352179120301496>

[5] G. M. Wallace, S. G. Baek, P. T. Bonoli, I. C. Faust, B. L. LaBombard, Y. Lin, R. T. Mumgaard, R. R. Parker, S. Shiraiwa, R. Vieira, D. G. Whyte, S. J. Wukitch, High field side launch of RF waves: A new approach to reactor actuators, *AIP Conference Proceedings* 1689 (1) (2015) 030017. arXiv:[https://pubs.aip.org/aip/acp/article-pdf/doi/10.1063/1.4936482/12873104/030017\\_1\\_online.pdf](https://pubs.aip.org/aip/acp/article-pdf/doi/10.1063/1.4936482/12873104/030017_1_online.pdf), doi:10.1063/1.4936482. URL <https://doi.org/10.1063/1.4936482>

[6] N. Smick, B. LaBombard, C. Pitcher, Plasma profiles and flows in the high-field side scrape-off layer in alcator c-mod, *Journal of Nuclear Materials* 337–339 (2005) 281–285, pSI-16. doi:<https://doi.org/10.1016/j.jnucmat.2004.09.035>. URL <https://www.sciencedirect.com/science/article/pii/S0022311504008979>

[7] N. Smick, B. LaBombard, I. Hutchinson, Transport and drift-driven plasma flow components in the alcator c-mod boundary plasma, *Nuclear Fusion* 53 (2) (2013) 023001. doi:10.1088/0029-5515/53/2/023001. URL <https://doi.org/10.1088/2F0029-5515%2F53%2F2%2F023001>

[8] B. LaBombard, A. Kuang, D. Brunner, I. Faust, R. Mumgaard, M. Reinke, J. Terry, J. Hughes, J. Walk, M. Chilenski, Y. Lin, E. Marmar, G. Wallace, D. Whyte, S. Wolfe, S. Wukitch, High-field side scrape-off layer investigation: Plasma profiles and impurity screening behavior in near-double-null configurations, *Nuclear Materials and Energy* 12 (2017) 139 – 147, proceedings of the 22nd International Conference on Plasma Surface Interactions 2016, 22nd PSI. doi:<https://doi.org/10.1016/j.nme.2016.10.006>. URL <http://www.sciencedirect.com/science/article/pii/S2352179116300400>

[9] P. N. Guzdar, J. F. Drake, D. McCarthy, A. B. Hassam, C. S. Liu, Three-dimensional fluid simulations of the nonlinear drift-resistive ballooning modes in tokamak edge plasmas, *Physics of Fluids B: Plasma Physics* 5 (10) (1993) 3712–3727. doi: 10.1063/1.860842.

[10] M. V. Umansky, X. Q. Xu, B. Dudson, L. L. LoDestro, J. R. Myra, Status and verification of edge plasma turbulence code bout, *Computer Physics Communications* 180 (6) (2009) 887–903. doi:<https://doi.org/10.1016/j.cpc.2008.12.012>. URL <https://www.sciencedirect.com/science/article/pii/S0010465508004293>

[11] F. Chen, *Introduction to Plasma Physics and Controlled Fusion*, no. v. 1 in *Introduction to Plasma Physics and Controlled Fusion*, Springer, 1984. URL <https://books.google.com/books?id=ToAtqnznr80C>

[12] M. V. Umansky, B. I. Cohen, I. Joseph, Simulations of tokamak edge plasma turbulent fluctuations based on a minimal 3d model, *Plasma Physics and Controlled Fusion* 66 (4) (2024) 045015. doi:10.1088/1361-6587/ad2b91. URL <https://dx.doi.org/10.1088/1361-6587/ad2b91>

[13] B. D. Dudson, M. V. Umansky, X. Q. Xu, P. B. Snyder, H. R. Wilson, Bout++: A framework for parallel plasma fluid simulations, *Computer Physics Communications* 180 (9) (2009) 1467 – 1480. doi:<https://doi.org/10.1016/j.cpc.2009.03.008>. URL <http://www.sciencedirect.com/science/article/pii/S0010465509001040>

[14] A. E. Fraser, M. J. Pueschel, P. W. Terry, E. G. Zweibel, Role of stable modes in driven shear-flow turbulence, *Physics of Plasmas* 25 (12) (2018) 122303. arXiv:[https://pubs.aip.org/aip/pop/article-pdf/doi/10.1063/1.5049580/19794000/122303\\_1\\_online.pdf](https://pubs.aip.org/aip/pop/article-pdf/doi/10.1063/1.5049580/19794000/122303_1_online.pdf), doi:10.1063/1.5049580. URL <https://doi.org/10.1063/1.5049580>

## 7. Figure captions

Figure 1: The slab domain representing SOL. The coordinates  $x, y, z$  shown are the field-aligned coordinates used in the calculation.

Figure 2: Normalized DRBM growth rate  $\hat{\omega}$  vs. the nondimensional parameter  $\xi_{\perp} = k_{\perp} \rho_{ci}$  for several different values of parameters  $\mathcal{A}, \mathcal{B}$  defined in the main text.

Figure 3: Data points from linear simulations shown with corresponding analytic results for the wavenumber scan.

Figure 4: Scaling of turbulent radial density flux with the density scale length. The symbols show results from the simulations, the dashed line shows the power-law fit and dot-dashed line shows the exponential fit explained in the main text.

Figure 5: The probability density function (PDF) of the radial density flux for different values of the density scale length  $L_n$ .

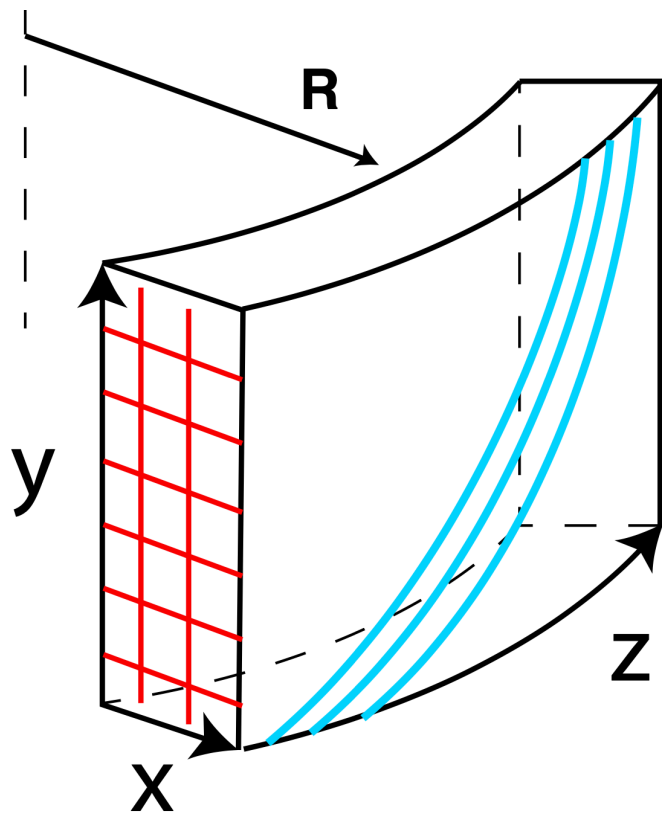


Fig. 1

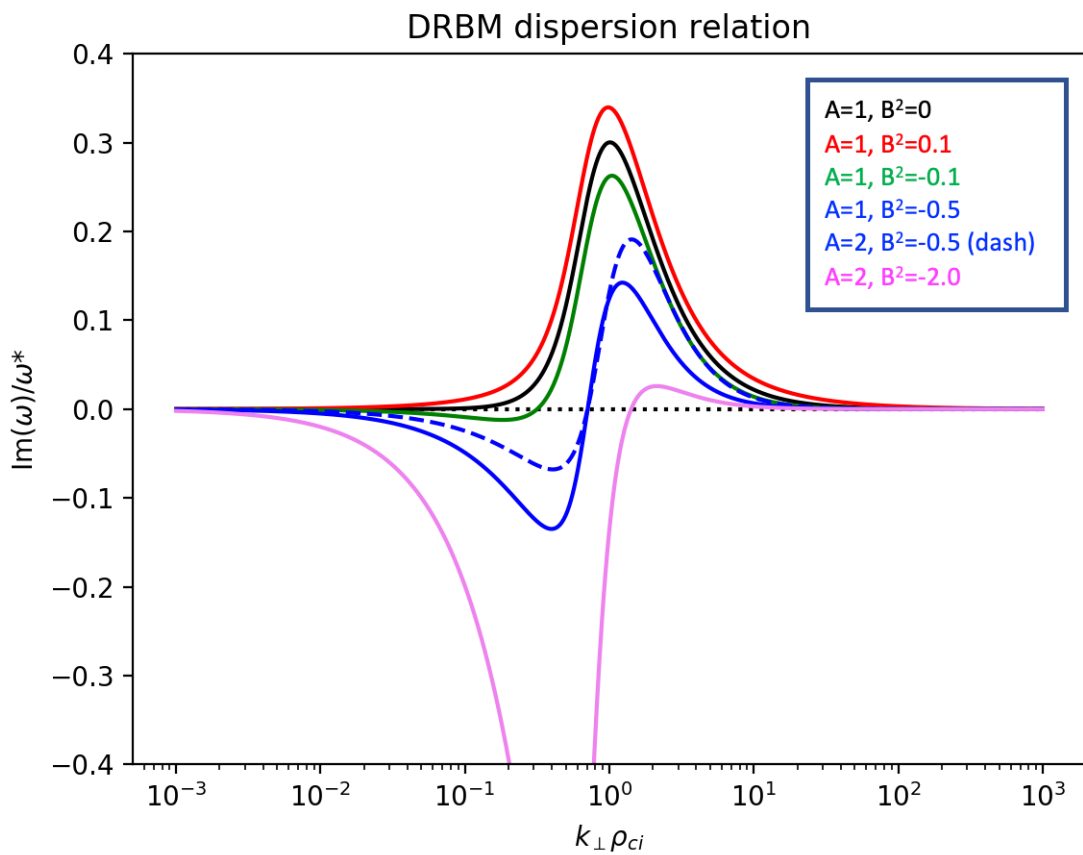


Fig. 2

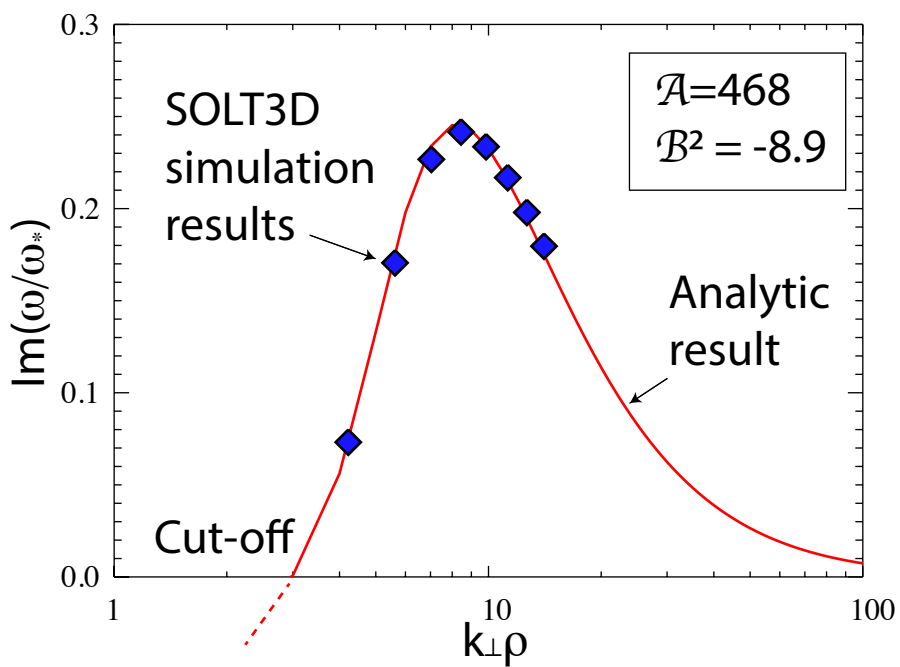


Fig. 3

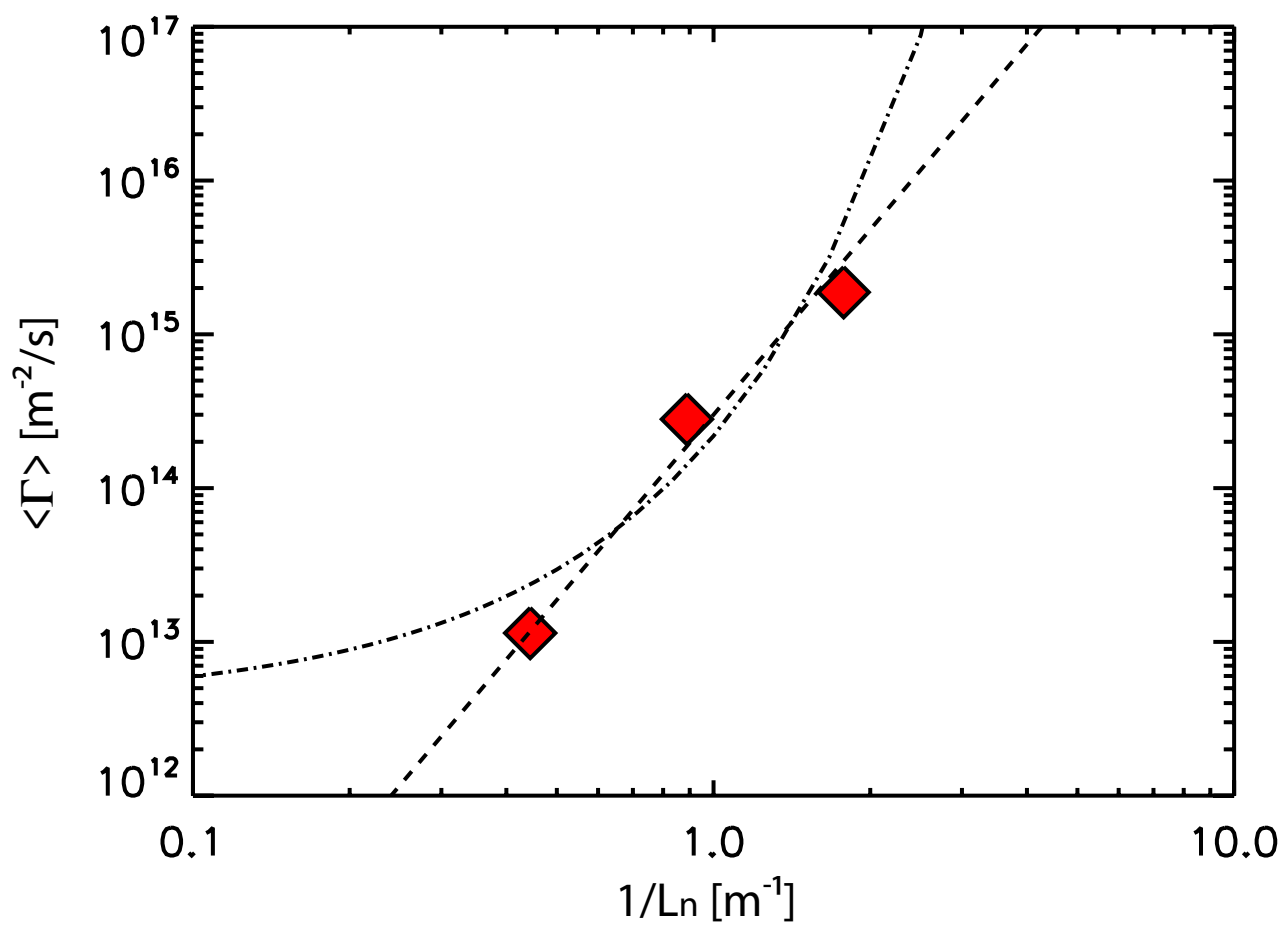


Fig. 4

Fig. 5

Normalized probability density for  $\Gamma$

